nature communications

Article

https://doi.org/10.1038/s41467-025-57411-7

The ARC^{CRABP1} neurons play a crucial role in the regulation of energy homeostasis

Received: 29 April 2024

Accepted: 19 February 2025

Published online: 08 March 2025

Check for updates

Lihong Yan[1,2,3,9], Xin Zhang[1,2,9], Liling Jin[1,2], Yin Li[1,2], Yang Chen[1,2], Jubiao Zhang[1,2], Zhenning Sun[1,2], Junxia Qi[1,2], Changqing Qu[4], Guanzhong Dong[3], Yongjie Zhang[5], Qin Jiang[6] ✉, An Liu[7] ✉ & Juxue Li[1,2,6,8] ✉

Recent single-cell RNA sequencing study suggested that CRABP1 expressing neurons in the arcuate nucleus (ARC^{CRABP1} neurons) were a distinct group of neurons. However, the physiological role of ARC^{CRABP1} neurons remains unexplored. Here, we demonstrated that ARC^{CRABP1} neurons played a crucial role in regulation of energy homeostasis in male mice. Ablation of ARC^{CRABP1} neurons resulted in obesity and a diabetic phenotype in mice. By employing chemogenetic or optogenetic manipulation techniques, the inhibition and activation of ARC^{CRABP1} neurons resulted in an increase and decrease in food intake, respectively. The axon terminals from these ARC^{CRABP1} neurons project to several brain regions implicated in feeding regulation such as PVH, BNST, PBN, and NTS. Optogenetic manipulation of these axons within these brain regions resulted in significant alterations of food intake behavior in mice. Furthermore, the electrophysiological studies demonstrated that the activation of ARC^{CRABP1} neurons induces depolarization in POMC neurons in the hypothalamus. The hormone stimulation studies showed that most of the ARC^{CRABP1} neurons respond to insulin. Collectively, our findings demonstrate that ARC^{CRABP1} neurons represent a distinct neuronal subtype involved in energy homeostasis regulation.

The hypothalamus is a highly conserved brain region that governs vital physiological functions, including energy balance, growth, and reproduction[1–4]. Within this brain region, specific nuclei and neuronal circuits have been identified and extensively studied for their functional roles in regulating fundamental bodily processes[5,6]. Among these nuclei, the arcuate nucleus (ARC) plays a pivotal role in sensing and integrating peripheral signals to maintain energy homeostasis[7–9]. The anorexigenic proopiomelanocortin (POMC)-expressing neurons and orexigenic agouti-related peptide (AgRP)/neuropeptide Y(NPY)–expressing neurons are situated within the ARC of the hypothalamus and have been established as pivotal regulators of energy balance over the past three decades[7,10–14]. However, it is still uncertain whether there are additional undiscovered neuronal subtypes in the ARC that significantly impact the regulation of energy balance.

[1]State Key Laboratory of Reproductive Medicine and Offspring Health, Nanjing Medical University, Nanjing, Jiangsu 211166, China. [2]Jiangsu Provincial Key Laboratory of Molecular Targets and Intervention of Metabolic Disease, Nanjing, Jiangsu 211166, China. [3]The Second People's Hospital of Changzhou, the Third Affiliated Hospital of Nanjing Medical University, Changzhou Medical Center, Nanjing Medical University, Changzhou 213003, China. [4]Fuyang Normal University, Engineering Technology Research Center of Anti-aging Chinese Herbal Medicine, Fuyang, Anhui 236037, China. [5]Department of Human Anatomy of Nanjing Medical University, Human Brain Tissue Resource Center of Nanjing Medical University, National Health and Disease Human Brain Tissue Resource Center — sub-center of Nanjing Medical University, Nanjing, Jiangsu 211166, China. [6]The Affiliated Eye Hospital, Nanjing Medical University, Nanjing, Jiangsu 210029, China. [7]The Key Laboratory of Developmental Genes and Human Disease, Ministry of Education, The School of Life Science and Technology, Southeast University, 2 Sipailou Road, Nanjing 210096, China. [8]The Second Affiliated Hospital of Nanjing Medical University, Nanjing, Jiangsu 210011, China. [9]These authors contributed equally: Lihong Yan, Xin Zhang. ✉e-mail: jiangqin@njmu.edu.cn; liu_an@seu.edu.cn; lijuxue@njmu.edu.cn

In recent years, high-throughput single-cell transcriptome sequencing technology has provided a robust method for identifying distinct neuronal subtypes in the hypothalamus. A recent study conducted single-cell profiling in the adult mouse hypothalamus and discovered a distinct population of neurons expressing cellular retinoid-binding protein 1 (CRABP1) within the ARC (ARC^{CRABP1} neurons)[15]. Bioinformatics analyses revealed that ARC^{CRABP1} neurons did not co-express any known neuronal markers in ARC, indicating their classification as a distinct neuronal subtype[15]. CRABP1 is a highly conserved cytosolic protein that is expressed in various cell types, including adipocytes, motor neurons, and embryonic stem cells[16–19]. It functions as an integral component of the retinoic acid (RA) signaling pathway, exerting precise control over RA bio-availability through its high-affinity binding to RA[20,21]. The ARC^{CRABP1} neurons were reported to exhibit sensitivity to metabolic conditions[22]. Furthermore, another study revealed that *Crabp1* knockout mice displayed an obesity-prone phenotype in both chow feeding and high-fat diet feeding[23], prompting us to investigate the potential involvement of ARC^{CRABP1} neurons in energy homeostasis.

In this study, we have characterized the ARC^{CRABP1} neurons and confirmed that these neurons represent a distinct neuronal subtype in the hypothalamus. Through cell ablation studies, chemogenetic and optogenetic manipulations, as well as electrophysiological studies, we have provided compelling evidence that supports an essential role for ARC^{CRABP1} neurons in governing energy homeostasis and food intake. The ARC^{CRABP1} neurons could potentially serve as a distinct target for mechanistic research and clinical studies on obesity.

Results

ARC^{CRABP1} neurons represent a distinct neuronal group in the hypothalamus

To characterize the expression of *Crabp1* in the brain, we quantified both mRNA and protein levels of *Crabp1* in various brain regions of adult male mice. Interestingly, the expression of *Crabp1* was predominantly observed in the hypothalamus, with minimal to no expression detected in other examined brain regions or peripheral tissues. (Supplementary Fig. 1a–e). Subsequently, immunostaining was performed to validate the expression of CRABP1, specifically within the adult hypothalamus. A distinct population of cells expressing CRABP1 was identified in the ARC (Supplementary Fig. 2a), which is consistent with the ISH data from the Allen Mouse Brain Atlas[24] (Supplementary Fig. 2b). And we also delineated the distribution of CRABP1-expressing cells between anterior-posterior coordinates ranging from −0.94 to −2.70 mm relative to bregma (Supplementary Fig. 2c, d).

The CRABP1-expressing cells exhibited neuronal marker NeuN expression, while lacking expression of other cell markers such as astrocyte marker GFAP and neural stem cell marker Nestin (Supplementary Fig. 3a–c), thereby representing a population of neurons. Additionally, we confirmed the absence of co-expression between CRABP1 and some known neuronal subtype markers such as POMC, AgRP, kisspeptin (Kiss1), tyrosine hydroxylase (TH), somatostatin (SST), and cocaine- and amphetamine-regulated transcript protein (CARTPT) (Fig. 1a–f), suggesting their classification as a distinct class of hypothalamic neurons. Due to the hypothalamus is an evolutionary conserved brain region, we also examined whether CRABP1 expressing neurons (ARC^{CRABP1} neurons) exist in ARC of other species. Our results showed that ARC^{CRABP1} neurons are present in multiple species, including mouse, rats, and humans (Supplementary Figs. 2a, 4a, b). Together, we conclude that ARC^{CRABP1} neurons was a type of distinct neuronal group in the hypothalamus.

Ablation of ARC^{CRABP1} neurons cause an obese and diabetic phenotype in mice

To explore the function of ARC^{CRABP1} neurons, we employed a loss-of-function approach using our newly constructed *Crabp1-Cre* mice model (Supplementary Fig. 5a–c). The specificity of Cre expression was verified by injection of AAV-DIO-mCherry virus in ARC (Supplementary Fig. 5d). The immunofluorescence staining results showed that most mCherry positive cells in ARC were co-stained with CRABP1, indicating that specific Cre recombination in *Crabp1-Cre* mice (Supplementary Fig. 5e, f).

Next, we bilaterally injected a Cre-dependent AAV encoding activated caspase3 (AAV-DIO-Caspase3) or control AAV virus (AAV-DIO-mCherry) into the ARC of 8 weeks old male *Crabp1-Cre* mice (Fig. 2a). The expression of caspase3 in cells will lead to cell apoptosis, which was wildly used in cell ablation studies[25–28]. As expected, after 3 weeks of surgery recovery, the CRABP1 expression was not detected in the ARC of AAV-DIO-Caspase3 injected mice by our immunofluorescence staining assay, indicating the successful establishment of ARC CRABP1 expressing neurons ablation (ACENA) mouse model (Fig. 2b).

The ACENA mice and control mice were both fed a chow diet, and various metabolic indices were examined throughout the experiments. The ACENA mice showed significant increases in body weight and food intake than that of control mice after 10 weeks of chow feeding (Fig. 2c–e). The body composition analysis revealed that body weight gain attributed to an increase in fat mass but not in lean mass (Fig. 2f). Nevertheless, the energy expenditure of the ACENA mice were not significantly changed as compared to that of control mice, implying that the body weight gain of ACENA mice were attributed to increase of food intake but not to the reduction of energy expenditure (Fig. 2g–j). Furthermore, the ACENA mice exhibited elevated levels of serum leptin, insulin and impaired glucose tolerance (Fig. 2k–n). Consistent with body weight change, subcutaneous white adipose tissue (SC-WAT) adipocyte size, and hepatic lipid deposition were all increased in the ACENA mice as compared to controls (Fig. 2o). Together, the ACENA mice showed a typical obese phenotype, indicating that ARC^{CRABP1} neurons play an important role in energy metabolism.

ARC^{CRABP1} neurons regulate feeding

To explore the role of ARC^{CRABP1} neurons in feeding, we deployed the chemogenetic strategy to activate or inhibit the ARC^{CRABP1} neurons. The Gq-coupled designer receptor exclusively activated by designer drug (DREADD) (hM3Dq) is used to enhance neuronal activity, whereas the Gi/o-coupled DREADD (hM4Di) is utilized to inhibit neuronal activity. We bilaterally injected AAV enabling cre-dependent expression of hM3Dq (AAV-DIO-hM3Dq), hM4Di (AAV-DIO-hM4Di), or AAV-DIO-mCherry into ARC of the 8 weeks old male *Crabp1-Cre* mice (Fig. 3a). After 3 weeks of surgery recovery, the AAV virus injected mice were administered with DCZ intravenously and measured food intake for 4 hours. As shown in Fig. 3b–d, activation of hM3Dq in ARC^{CRABP1} neurons by DCZ resulted in a significant reduction of food intake in AAV-DIO-hM3Dq injected mice as compared to that of control mice. In contrast, inhibition of hM4Di in ARC^{CRABP1} neurons by DCZ led to a significant increase in food intake in AAV-DIO-hM4Di injected mice as compared to that of control mice (Fig. 3e–g).

Next, we performed optogenetic studies to assess the functional role of ARC^{CRABP1} neurons in feeding. We bilaterally injected the AAV enabling Cre-dependent expression of channelrhodopsin-2 (ChR2) (AAV-DIO-ChR2-mCherry), natronomonas halorhodopsin (NpHR) fused to mCherry (AAV-DIO-NpHR-mCherry), or AAV-DIO-mCherry into ARC of the 8 weeks old male *Crabp1-Cre* mice. After 3 weeks of surgery recovery, an optical fiber with an electrode was placed close to the original virus injection site (Fig. 3a). After surgery recovery, the activities of ARC^{CRABP1} neurons in AAV virus mice were manipulated by activated with a blue light (470 nm) or inhibited with a yellow light (593 nm). Consistent to the chemogenetic results, activation of ARC^{CRABP1} neurons significantly reduced the food intake of AAV-DIO-ChR2-mCherry injected mice as compared to that of control mice (Fig. 3h–j). Inhibition of ARC^{CRABP1} neurons significantly increased the food intake of AAV-DIO-NpHR-mCherry injected mice as compared

https://doi.org/10.1038/s41467-025-57411-7

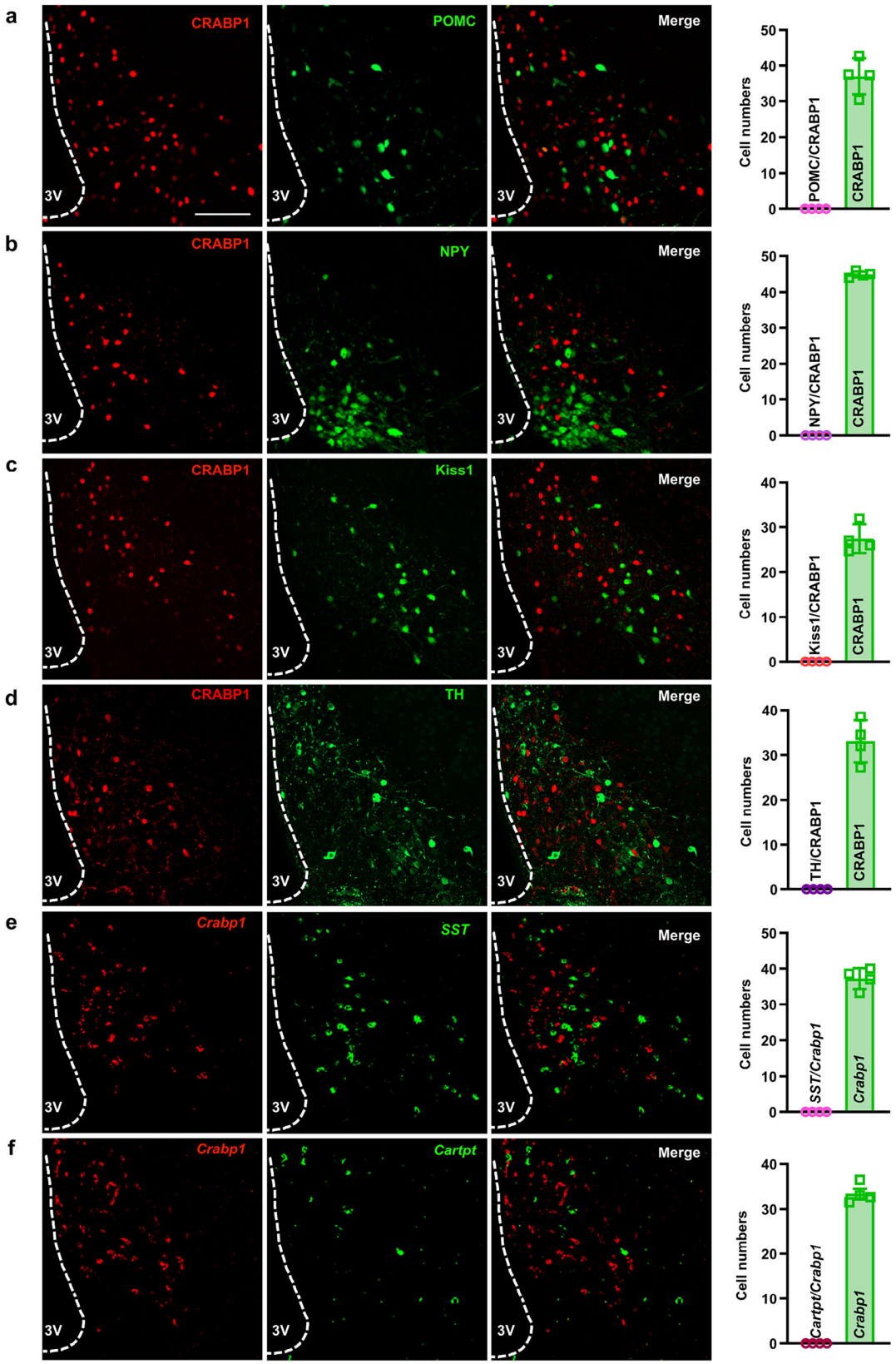

Fig. 1 | The ARC^{CRABP1} neurons did not express makers of other known neuronal subtypes in ARC. a–d Representative confocal images and statistical results depicting the immunofluorescence co-localization of CRABP1 (red) with neural subtype markers (green), including POMC, NPY, Kiss1, and TH in the ARC region. ($n = 4$). **e**, **f** The representative FISH images and statistical results depicting the co-localization of *Crabp1* mRNA (red) with *Sst* mRNA (green) and *Cartpt* mRNA (green). ($n = 4$). *n* represents mice number. Scale bar, 100 μm.

https://doi.org/10.1038/s41467-025-57411-7

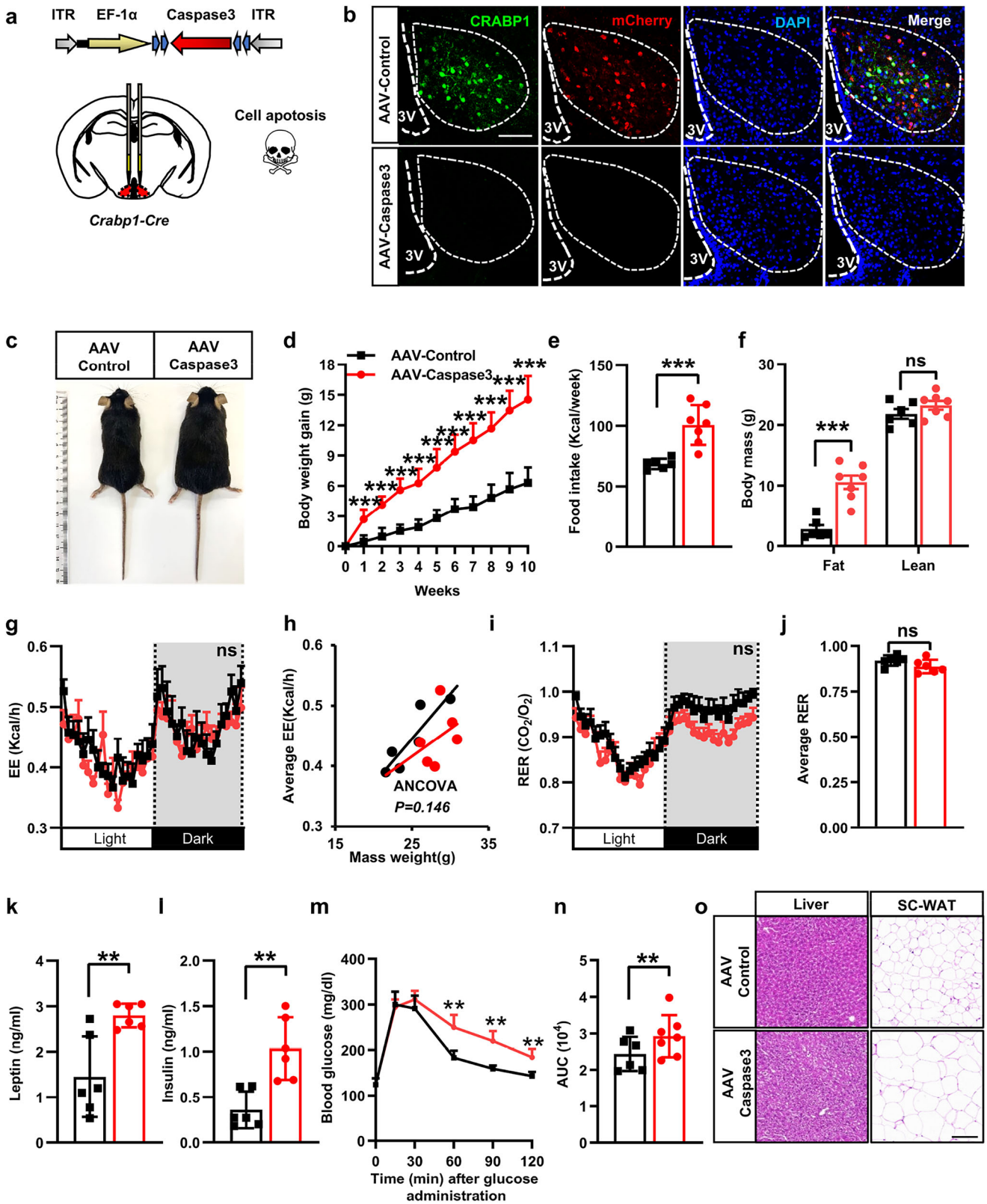

to that of control mice (Fig. 3k–m). Altogether, we conclude that ARC^{CRABP1} neurons play an important role in food intake regulation.

Projection of ARC^{CRABP1} neurons from ARC to other feeding-regulating brain regions

Firstly, we employed classical anterograde and retrograde tracing techniques to investigate the downstream targets of ARC^{CRABP1} neurons throughout the entire brain. For the anterograde tracing assay, we bilaterally injected AAV-DIO-TK-GFP into the hypothalamus of *Crabp1-Cre* mice. Three weeks after the AAV-DIO-TK-GFP injection, we administered HSV-ΔTK-tdTomato into the same injection site (Fig. 4a, b). Our findings revealed that tdTomato-positive neurons were distributed across various brain regions including caudate nucleus (CPU), the ventral lateral septum (LSV), the bed nucleus of the stria terminalis

Fig. 2 | The ACENA mice show an obesity and diabetic phenotype. a Schematic illustration of AAV-Ef1a-DIO-Caspase3 injection into the ARC of *Crabp1-Cre* mice. **b** Representative image of immunofluorescence staining of CRABP1 (green) in ARC of both control mice and ACENA mice. mCherry: red; DAPI: blue. Scale bar, 100 μm. **c** Representative image of ACENA mice and control mice after feeding on chow for 10 weeks. **d**–**n** Various metabolic indicators including body weight (**d**), food intake (**e**), fat mass and lean mass (**f**), energy expenditure (**g**), regression of energy expenditure with body mass (**h**), respiratory exchange ratio (**i**), average of respiratory exchange ratio (**j**), serum leptin level (**k**), serum insulin level (**l**), GTT (**m**), and AUC (**n**) were measured in both ACENA mice and control mice. Body weight (control: $n = 10$; ACENA: $n = 10$); other metabolic indicators (**e**, **f**, **m**, **n**, control: $n = 6$; ACENA: $n = 7$; **g**–**l**, control: $n = 6$; ACENA: $n = 6$). **o** Representative histology image of liver and WAT in both ACENA mice and control mice. ($n = 3$). Scale bar, 100 μm. *n* represents mice number. Results are presented as mean ± SEM. Statistic methods: Two-way ANOVA with Sidak's or Tukey's test (**d**, **f**, **m**), two-sided regression-based ANCOVA (**g**–**j**) and two-tailed Student's *t*-test (**e**, **k**, **i**, **n**). ns represents not significant, $^{*}P < 0.05$, $^{**}P < 0.01$, and $^{***}P < 0.001$.

(BNST), the paraventricular hypothalamic nucleus (PVH), the periaqueductal gray (PAG), parabrachial nucleus (PBN) and the nucleus tractus solitarius (NTS) (Fig. 4c). To further validate the projection target brain regions of ARC^{CRABP1} neurons, we bilaterally injected AAV-hSyn-DIO-mGFP-T2A-Synaptophysin-mRuby into the ARC region of adult male *Crabp1-Cre* mice (Supplementary Fig. 6a, b). Once again, we observed a concentration of synaptic vesicles expressing red fluorescence in CPU, LSV, BNST, PVH, PAG, PBN, and NTS (Supplementary Fig. 6c). Among these brain regions, PVH, BNST, PBN, and NTS have been reported to regulate feeding behavior[29–32]. Next, we conducted retrograde tracing to confirm projections from ARC^{CRABP1} neurons to these feeding behavior-related brain regions. We injected cholera toxin subunit B (CTB) conjugated with Alexa Fluor^{TM}555[33–35] into PVH, BNST, PBN, and NTS, respectively (Supplementary Fig. 7a–l). Immunofluorescence analysis demonstrated that CTB could be retrogradely transported to ARC^{CRABP1} neurons. In conclusion, the present study provides evidence for projections originating from ARC^{CRABP1} neurons to their downstream targets.

Food suppression upon optogenetic activation of ARC^{CRABP1} neurons

We explored the potential involvement of axon terminals of ARC^{CRABP1} neurons in the brain region of PVH, PBN, BNST, and NTS in feeding regulation by stereotaxically injecting AAV-DIO-ChR2-mCherry and AAV-DIO-NpHR-mCherry into the ARC (Fig. 5). Subsequently, we optogenetically stimulated axon terminals of ARC^{CRABP1} neurons in PVH, PBN, BNST, and NTS to examine their roles in feeding regulation. Activation of ARC^{CRABP1} neurons axon terminals in the BNST, PBN, and NTS resulted in a robust suppression of feeding behavior (Fig. 5a, c, d), while activation of terminals in the PVH had no effect on feeding behavior (Fig. 5b). Conversely, inhibition of PVN, PBN, and NTS significantly promoted feeding behavior (Fig. 5f–h), with no impact observed on feeding behavior within the BNST regions (Fig. 5e). These findings suggest that ARC^{CRABP1} neurons play a role in regulating feeding involved with specific brain regions including BNST, PVH, PBN, and NTS.

Optogenetic activation of ARC^{CRABP1} neurons excites POMC neurons

The AAV-DIO-mCherry viruses were injected into *Crabp1-Cre* mice for the purpose of labeling ARC^{CRABP1} neurons, NPY neurons were labeled using *NPY-hrGFP* mice, and POMC neurons were labeled using *POMC-eGFP* mice. Subsequently, patch-clamp recordings were conducted to assess their electrophysiological characteristics (Fig. 6a). As shown in Fig. 6b–d, ARC^{CRABP1} neurons displayed comparable resting membrane potentials (RMP), rheobase currents and membrane input resistance to those of NPY neurons and POMC neurons. Additionally, the amplitude and kinetic characteristics of their action potentials (APs) are also comparable (Fig. 6e–i). The previous studies have demonstrated the sensitivity of NPY neurons and POMC neurons to variations in environmental glucose levels[25,36]. We treated ARC^{CRABP1} neurons, NPY neurons, and POMC neurons with a low glucose concentration (3 mM) and found that reducing glucose levels also inhibited ARC^{CRABP1} neuronal activity (Fig. 6j–m). We also performed miniature excitatory postsynaptic current (mEPSC) recording, and found that the three kinds of neurons exhibited similar mEPSC amplitude and frequency (Supplementary Fig. 8a–c).To investigate potential functional connections between ARC^{CRABP1} neurons and NPY neurons and POMC neurons, we injected the AAV-DIO-ChR2-mCherry virus into *Crabp1-Cre*::*POMC-eGFP* mice to express ChR2 in ARC^{CRABP1} neurons and conducted patch-clamp recordings on POMC neurons, and simultaneously injected AAV-DIO-ChR2-mCherry and AAV-*fnpy*-GFP virus into *Crabp1-Cre* mice express ChR2 in ARC^{CRABP1} neurons and labeled NPY neurons with GFP to conduct patch-clamp recordings on NPY neurons (Fig. 6n). The results demonstrated that activating ARC^{CRABP1} neurons can lead to induce depolarization of POMC neurons, but not NPY neurons (Fig. 6o, p). Interestingly, the depolarization observed in POMC neurons could be inhibited by glutamate receptor inhibitors (CNQX + AP5), while GABA receptor inhibitors (PTX + CGP 52432) did not show any inhibitory effect (Fig. 6q). We further conducted perforated patch-clamp experiments to determine whether ARC^{CRABP1} neurons exhibit inward rectification in response to hyperpolarizing stimuli. Our findings revealed that 71.43% of ARC^{CRABP1} neurons displayed inward rectification, whereas only approximately one-third of NPY or POMC neurons exhibited this characteristic (Fig. 6r–t). Together, these findings suggest that ARC^{CRABP1} neurons can modulate POMC neuron activity by exerting influence on neighboring glutamatergic neurons or axons through neurotransmitters other than GABA.

ARC^{CRABP1} neurons respond to insulin stimulation

We explored the responses of ARC^{CRABP1} neurons to key metabolic hormones such as leptin, insulin, and ghrelin to better understand their roles in energy metabolism. By calculating the percentage of ARC^{CRABP1} neurons expressing phosphorylated signal transducer and activator of transcription-3 (p-STAT3), c-Fos (a marker of neuronal activation), and phosphorylated protein kinase B (p-AKT) following intracerebroventricular (ICV) injections of these hormones in mice, we identified distinct response patterns. Approximately 9% of ARC^{CRABP1} neurons were activated by leptin stimulation, as indicated by p-STAT3 expression (Fig. 7a–c). Insulin, on the other hand, elicited a robust response, with most of ARC^{CRABP1} neurons expressing p-AKT, suggesting that these neurons are highly sensitive to insulin (Fig. 7d–f). In contrast, few ARC^{CRABP1} neurons responded to ghrelin, as indicated by minimal c-Fos expression (Fig. 7g–i). These findings reveal a hormone-specific activation profile of ARC^{CRABP1} neurons, emphasizing their selective sensitivity to insulin over leptin and ghrelin.

Discussion

The hypothalamus acts as a central hub that integrates signals from different parts of the body to maintain energy homeostasis and ensure optimal functioning[37–39]. In the ARC of the hypothalamus, the POMC neurons and AgRP/NPY neurons were recognized as key neuronal populations which play essential roles in regulating feeding behavior and energy homeostasis[12,40–42]. Due to previous technical limitations, it remained unclear whether there are other significant distinct neuronal types within the hypothalamus involved in the regulation of energy metabolism. The emerging technology of single-cell sequencing has

https://doi.org/10.1038/s41467-025-57411-7

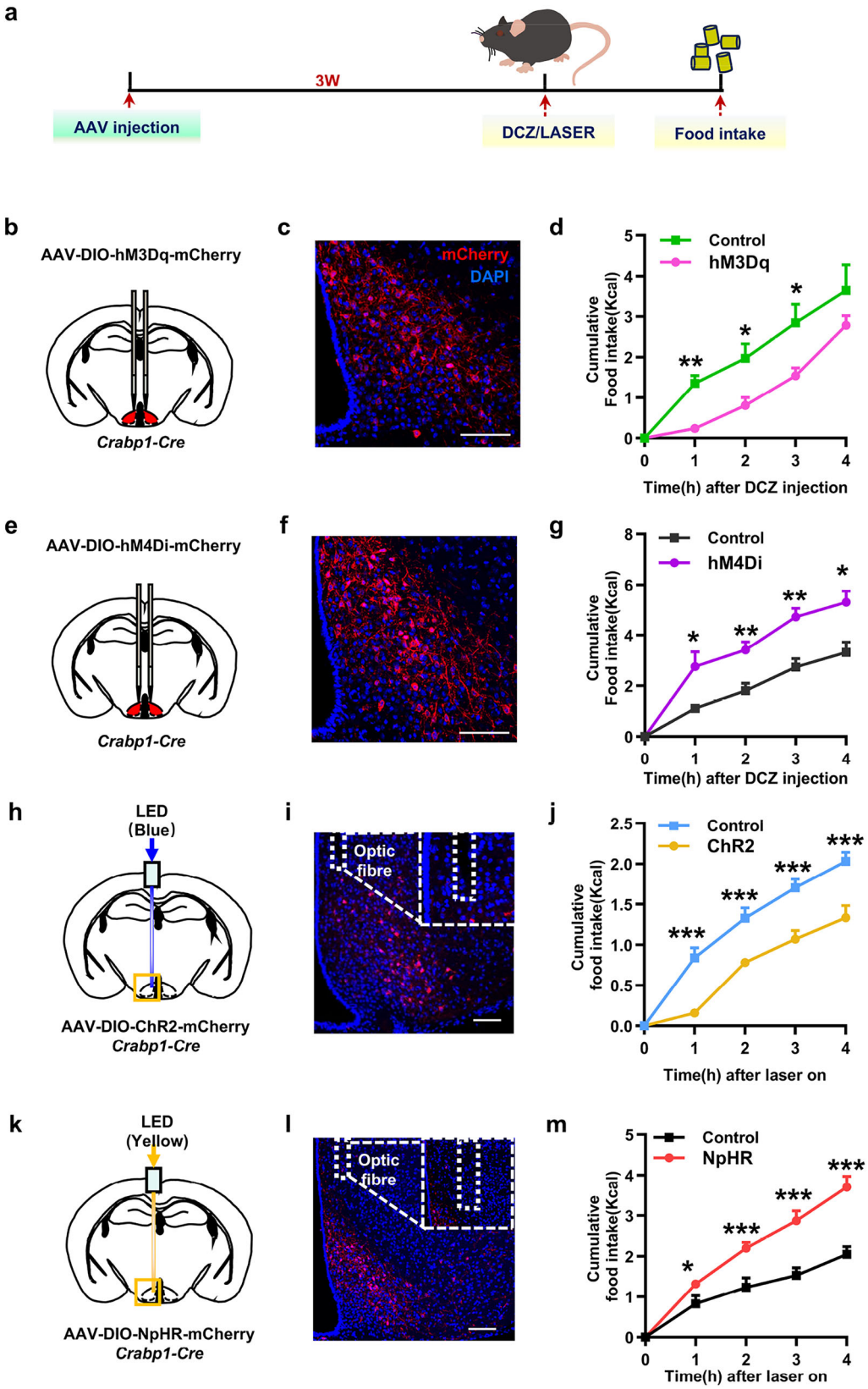

provided an unprecedented tool for the identification and characterization of distinct cell types in the hypothalamus. This has led to the discovery of ARC^{CRABP1} neurons through a study utilizing single-cell RNA-seq analysis[15]. The study, however, did not conduct experiments to validate its findings and establish the unique existence of this neuronal group in the hypothalamus. Therefore, we investigated the co-expression relationship between CRABP1 and other markers of known hypothalamic neuronal types. The absence of co-expression between CRABP1 and the established neural population markers in the ARC was confirmed through a series of immunostaining and FISH experiments, thus providing further evidence for its classification as a distinct cluster of neurons.

Fig. 3 | Modulation of ARC^{CRABP1} neurons activity influences food intake in mice. **a** Schematic illustration of modulation of ARC^{CRABP1} neurons by chemogenetic and optogenetic stimulation. **b**–**d** Representative image showed expression of hM3D (Gq) in ARC^{CRABP1} neurons as assessed by mCherry fluorescence (**c**). Cumulative food intake (**d**) was measured for 4 h after DCZ injection. (control: $n = 5$; hM3Dq: $n = 5$). **e**–**g** Representative image showed expression of hM4D (Gi) in ARC^{CRABP1} neurons as assessed by mCherry fluorescence (**f**). Cumulative food intake (**g**) was measured for 4 hours after DCZ injection. (control: $n = 5$; hM4Di: $n = 5$). **h**–**j** Representative image showed expression of ChR2 in ARC^{CRABP1} neurons as assessed by mCherry fluorescence as well as fiber placement (**i**). Cumulative food intake (**j**) was measured during 4 h with photostimulation. (control: $n = 5$; ChR2: $n = 5$). **k**–**m** Representative image showed expression of NpHR in ARC^{CRABP1} neurons as assessed by mCherry fluorescence as well as fiber placement (**l**). Cumulative food intake (**m**) was measured for 4 h with photostimulation. (control: $n = 5$; NpHR: $n = 5$). mCherry: red; DAPI: blue. *n* represents mice number. Scale bars, 100 μm. Data were expressed as mean ± SEM. Statistic methods: Two-way ANOVA with Sidak's or Tukey's test (**d**, **g**, **j**, **m**). $^{*}P < 0.05$, $^{**}P < 0.01$, and $^{***}P < 0.001$.

The hypothalamus is a highly conserved brain region where diverse neuronal populations are known to play pivotal roles in regulating various physiological processes of the body. The newly discovered ARC^{CRABP1} neurons are speculated to potentially play a pivotal role in the regulation of physiological processes within the body. However, its precise physiological function remains unexplored. The findings from a previous study have demonstrated that CRABP1 knockout mice exhibit a phenotype characterized by significantly increased body weight and food intake[23]. It is postulated that the functionality of ARC^{CRABP1} neurons may be intricately linked to energy metabolism. To test this hypothesis, we opted to ablate the population of ARC^{CRABP1} neurons in the hypothalamus of mice in order to ascertain whether it is indeed the mice that manifest an energy metabolism related phenotype. The exciting findings support our hypothesis that the ablation of ARC^{CRABP1} neurons in the hypothalamus leads to the manifestation of a typical obesity phenotype in mice. In addition to cell ablation experiments, optogenetic and chemogenetic methods have been widely used as crucial tools in the field of neuroscience for studying neuronal function[43]. The findings of our optogenetic and chemogenetic study indicate that ARC^{CRABP1} neurons play a crucial role in the regulation of food intake. It is noteworthy that previous studies on POMC neurons and AgRP/NPY neurons have employed these methods to substantiate their crucial roles in energy metabolism[44–47]. Therefore, this work provides strong evidence supporting the pivotal role of ARC^{CRABP1} neurons in energy metabolism.

Neuronal projections to specific brain regions allow them to carry out regulatory functions related to their specialized roles[5,32,48,49]. In order to identify the projection brain regions of ARC^{CRABP1} neurons, we performed HSV virus tracing study in *Crabp1-Cre* mice. ARC^{CRABP1} neurons were found to project to various brain regions, including the BNST, PVH, PBN, and NTS which have been implicated in the regulation of food intake. PVN neurons are crucial components in the neural circuitry involved in regulating feeding behavior and energy homeostasis by transmitting signals from excitatory AgRP/NPY neurons and POMC neurons to various target regions within the brain[31,50,51]. The PBN plays a crucial role in processing and integrating gustatory and visceral information, making it a vital transit station for regulating feeding behavior[32,52]. By receiving inputs from various sensory pathways, the PBN is able to decipher signals related to taste, smell, texture, and temperature of food. AgRP fiber projection into BNST can cause profound effects on food intake and reward[53,54]. Photogenetic activation of AgRP fibers in BNST can evoke food intake in fed mice and activate GABAergic nerves, so that efferent projection of BNST to LHA can induce eating and reward-related behaviors[30]. Stimulation of BNST-projected AgRP neurons can induce feeding behavior[55]. NTS is a crucial region in the brainstem that plays a significant role in regulating food intake through receiving signals transmitted by POMC neurons[29,56–58]. The projection of ARC^{CRABP1} neurons into these brain regions suggests that they may exert their regulatory function on feeding through these specific neural pathways. Interestingly, optogenetic stimulation of ARC^{CRABP1} neurons in these specific brain regions elicits a robust response in feeding behavior, providing compelling evidence for ARC^{CRABP1} neurons in regulating feeding through these neural circuits. This technology is still relatively reliable and preferred at present. However, axon collateralization of ARC^{CRABP1} neurons in these brain regions cannot be ruled out, as the feeding phenotypes resulting from optogenetic activation in these brain regions were similar in our study. We will explore this question in our future research endeavors.

Our electrophysiological studies revealed that ARC^{CRABP1} neurons exhibited characteristics similar to those observed in the established electrophysiological profiles of POMC and AgRP/NPY neurons. Additionally, we observed that ARC^{CRABP1} neurons exhibit glucose sensitivity comparable to that of POMC and AgRP/NPY neurons. Importantly, we discovered that optogenetic activation of ARC^{CRABP1} neurons led to the excitation of POMC neurons, potentially explaining the observed feeding behaviors in our mouse models. Previous study has demonstrated that ARC^{CRABP1} neurons are often GABAergic in nature[59]. Hence, our findings propose the potential regulation of POMC neurons activity by ARC^{CRABP1} neurons might be through their influence on adjacent glutamatergic neurons or axons via neurotransmitters other than GABA, thereby orchestrating a sophisticated interplay within the neural network.

POMC and AgRP neurons in the hypothalamus play a crucial role in maintaining energy balance by sensing fluctuations in key metabolic hormones such as leptin, insulin, and ghrelin. Leptin suppresses food intake and increases energy expenditure by targeting POMC and AgRP neurons through the Janus-activated kinase (JAK)-2 -STAT3 pathway[60,61]. Our findings show that only a small fraction of ARC^{CRABP1} neurons exhibit STAT3 phosphorylation in response to leptin, indicating limited sensitivity to leptin stimulation. Insulin regulates whole-body glucose metabolism and elicits anorectic effects by activating POMC neurons and inhibiting AgRP/NPY neurons via the Irs-phosphoinositide 3-kinase (PI3K)-Akt pathway[62,63]. Notably, insulin robustly induces AKT phosphorylation in most ARC^{CRABP1} neurons, highlighting their selective responsiveness to insulin stimulation. Ghrelin activates orexigenic AgRP neurons and enhances inhibitory GABAergic inputs onto anorexigenic POMC neurons, promoting food intake[47,64,65]. However, ARC^{CRABP1} neurons are unresponsive to ghrelin stimulation. Collectively, our findings showed that ARC^{CRABP1} neurons exhibited a distinct response pattern to key metabolic hormones. ARC^{CRABP1} neurons may play a selective role in insulin-driven metabolic regulation, warranting further research to explore its molecular mechanism and physiological role in insulin-mediated energy homeostasis.

In conclusion, we revealed that ARC^{CRABP1} neurons are a distinct neuronal population, which are crucially involved in the regulation of energy metabolism. The identification of ARC^{CRABP1} neurons provides an opportunity for mechanistic research and clinical studies aimed at combating obesity. In future studies, we aim to investigate the role of insulin in ARC^{CRABP1} neurons in mediating metabolic regulation and to explore the involvement of CRABP1 in regulating energy metabolism via these neurons.

Methods

Human samples

The postmortem human hypothalamic tissues (from three male individuals, aged 79, 50, and 95) were obtained from the Human Anatomy Department of Nanjing Medical University. The utilization of human

https://doi.org/10.1038/s41467-025-57411-7

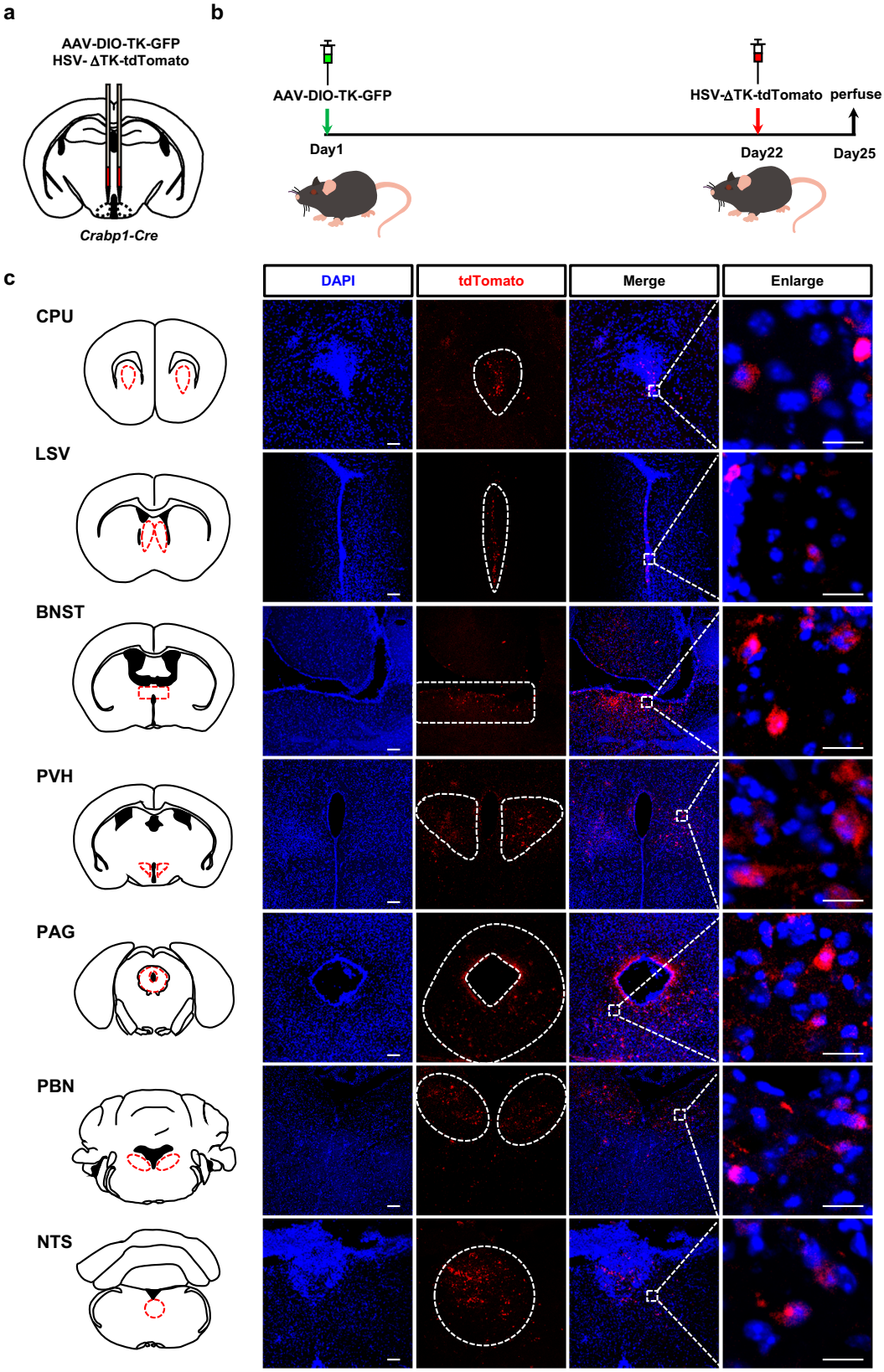

Fig. 4 | ARC^{CRABP1} neurons project to various brain regions. a, **b** A Schematic illustration of the virus injection (AAV-EF1α-DIO-EGFP-T2A-TK and HSV-ΔTK-LSL-tdTomato) into the ARC of *Crabp1-Cre* mice. **c** ARC^{CRABP1} neurons projection fields (Left). Representative fluorescent images of the brain regions, including CPU, LSV, BNST, PVH, PAG, PBN, and NTS, reveal tdTomato-labeled downstream neurons of ARC^{CRABP1} neurons ($n = 4$). Enlarged the output neurons labeled by tdTomato from ARC^{CRABP1} neurons are depicted on the right. tdTomato: red; DAPI: blue. CPU caudate nucleus, LSV ventral lateral septum, BNST the bed nucleus of the stria terminalis, PVH paraventricular hypothalamic nucleus, PAG periaqueductal gray, PBN parabrachial nucleus, NTS nucleus tractus solitarius. *n* represents mice number. Scale bars, 100 and 20 μm (Enlarge panel).

https://doi.org/10.1038/s41467-025-57411-7

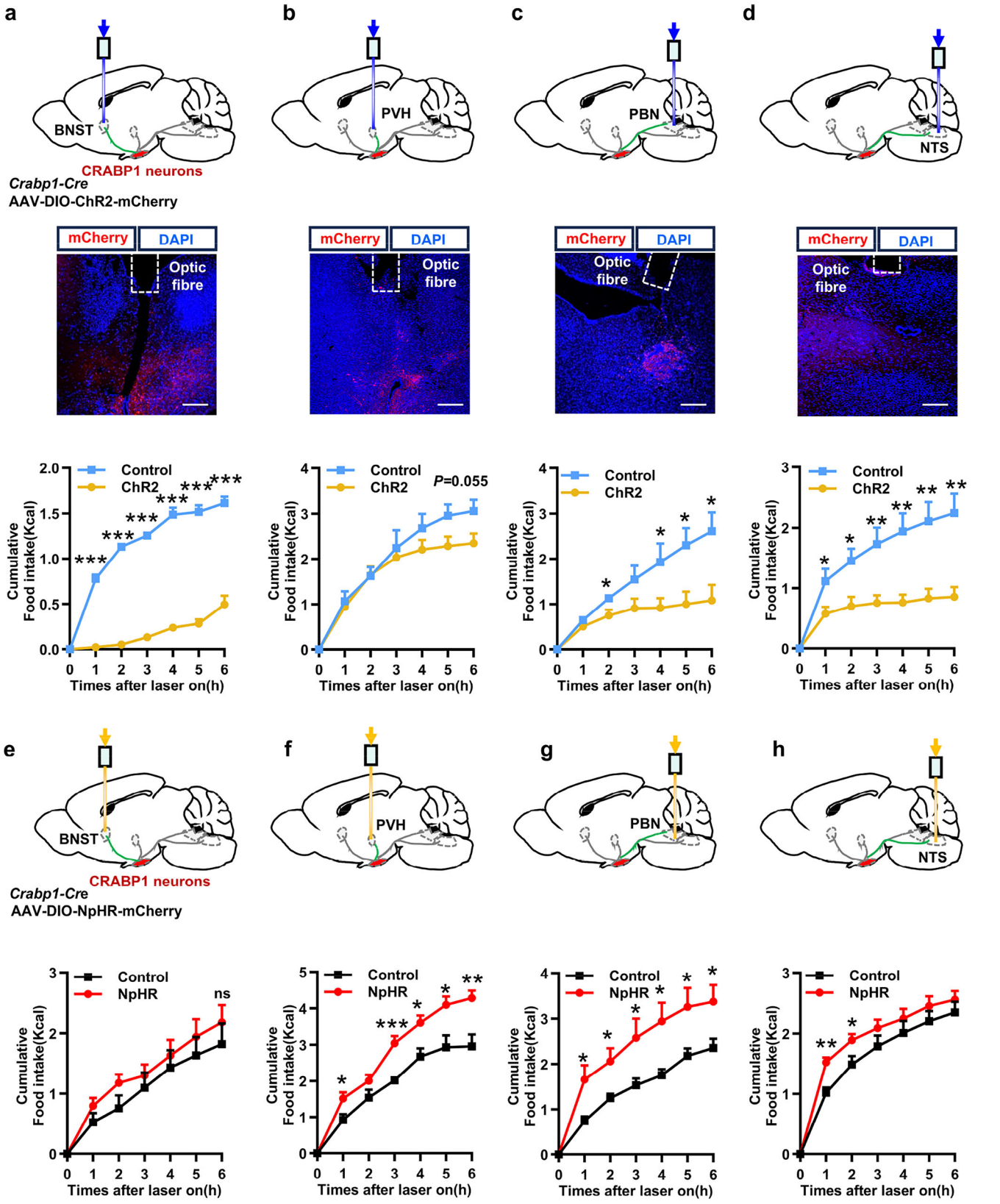

brain tissues adhered to a protocol approved by the Ethics Review Committee of Nanjing Medical University of Review Board (2022816).

Animals

Pomc-eGFP, *NPY-hrGFP*, *Kiss1-Cre*, and *Rosa26-EYFP* mice in C57BL/6J background were purchased from Jackson Laboratory (USA). *Nestin-GFP* mice in C57BL/6J background were purchased from Saiye Biotechnology (Guangzhou, China). Wild-type C57BL/6J mice and Spraque-Dawley rat were purchased from the Laboratory Animal Center of Nanjing Medical University. All experiments were conducted using male animals. All animal procedures were conducted in compliance with protocols approved by the Institutional Animal Care and

Fig. 5 | ARC^{CRABP1} neurons' axon terminals in BNST, PVN, PBN, and NST regulate food intake. a–d Top, diagrams depict optogenetic stimulation of axon terminals of ARC^{CRABP1} neurons following injection with AAV-hSyn-DIO-mCherry or AAV-DIO-ChR2-mCherry. Middle, the representative image showed ChR2 expression (red fluorescence) in ARC^{CRABP1} neurons fibers within the BNST, PVN, PBN, and NTS. ($n = 4$). DAPI: blue. Bottom, cumulative food intake was measured over a 6-h period during photostimulation. BNST (control: $n = 7$; ChR2: $n = 7$), PVH (control: $n = 6$; ChR2: $n = 6$), PBN (control: $n = 6$; ChR2: $n = 7$), NTS (control: $n = 7$; ChR2: $n = 7$). **e–h** Top, diagrams depict optogenetic inhibition of axon terminals of ARC^{CRABP1} neurons following injection with AAV-hSyn-DIO-mCherry or AAV-DIO-NpHR-mCherry. Bottom, cumulative food intake was measured over a 6-h period during photostimulation. BNST (control: $n = 7$; NpHR: $n = 7$), PVH (control: $n = 6$; NpHR: $n = 6$), PBN (control: $n = 6$; NpHR: $n = 6$), NTS (control: $n = 7$; NpHR: $n = 7$). n represents mice number. Scale bars, 100 μm. Data were expressed as mean ± SEM. Statistical methods: Two-way ANOVA with Sidak's or Tukey's test. ns represents not significant, $^{*}P < 0.05$, $^{**}P < 0.01$, $^{***}P < 0.001$.

Use Committee of Nanjing Medical University. Permission to maintain and breed mice was issued by the Laboratory Animal Center of Nanjing Medical University. Mice were housed in individually ventilated cages (IVCs) at 20–24 °C using a 12-h light/dark cycle. Animals had access to water and food ad libitum. Food was only withdrawn if required for an experiment during defined fasting periods.

Construction of *Crabp1-P2A-Cre* mice

Crabp1-P2A-Cre mice were generated by Saiye Biotechnology (Guangzhou, China). To create *Crabp1-Cre* knock-in mice, a targeting vector was designed to replace the TAA stop codon in the fourth exon of the *Crabp1* gene with *P2A-Cre*. The donor vector containing the "*P2A-Cre*" cassette was used to insert between the PCR-amplified left arm of homology (LAH) and right arm of homology (RAH). The 2.4 kb LAH was amplified from the bacterial artificial chromosome (BAC) of C57BL/6J mice using oligos 5′ arm forward primer: GATAGGGCATTTGTC-TAGTTCAG and 3′ knock in (KI) reverse primer: TTTCGGCTA-TACGTAACAGGGTGT. Additionally, the 2.7 kb RAH was amplified from BAC of C57BL/6J mice using oligos 5′ KI forward primer: CCAGC-TAAACATGCTTCATCGT and 3′ arm reverse primer: ATAT-CAATCTGGGACCTCTCCAT. The LAH and RAH were inserted into the donor vector containing the "*P2A-Cre*" cassette. The gRNA: TTTATGTCCGGGAGTAAAGG targeted mouse *Crabp1* gene, along with the donor vector containing the "*P2A-Cre*" cassette and Cas9 mRNA, were co-injected into fertilized mouse eggs to generate targeted knock-in offspring. F0 founder animals were identified by PCR followed by sequence analysis, which were bred to wild-type mice for germline transmission and F1 animal generation.

Immunohistochemistry

For immunohistochemistry assays, adult male mice or rats were deeply anesthetized and transcardially perfused with phosphate-buffered saline (PBS), followed by 4% paraformaldehyde (PFA). The brains were then post-fixed for 8 h at 4 °C. Subsequently, the brains were transferred to PBS containing 20% and 30% sucrose for gradient dehydration at 4 °C until they sank. Finally, the frozen brains were sectioned using a cryostat at −20 °C, with each section being ~20-μm thick. These sections were processed for immunofluorescence as described below.

Brain sections underwent three washes of 5 min each with PBS (0.1 M; pH 7.4) were then incubated in a blocking solution consisting of PBS containing 0.3% Triton X-100 and 5% goat serum for 1 h at room temperature. Following this, the sections were incubated overnight at 4 °C with primary antibodies including anti-CRABP1 (12588-1-AP, Proteintech; 13163, Cell Signaling Technology; GTX22816, Gene Tex), anti-NeuN (MAB377, Millipore), anti-GFAP (3670, Cell Signaling Technology), anti-TH (25859-1-AP, Proteintech), p-AKT (4460, Cell Signaling Technology), p-STAT-3 (9145, Cell Signaling Technology), and c-Fos (2250, Cell Signaling Technology).

After washing five times with PBS for 5 min each time, the sections were then incubated with secondary antibodies Alexa Fluor®488/555/647 conjugates against rabbit or mouse IgG diluted to a concentration of 1:1000 in Thermo Fisher's antibody dilution buffer for 1 h at room temperature while protected from light. The slides were washed five times with PBS before being mounted using a DAPI mounting medium. Images were acquired using an LSM800 confocal microscope manufactured (Carl Zeiss, Germany) and subsequently analyzed.

For 3, 3′-diaminobenzidine (DAB) staining, paraffin-embedded sections of formalin-fixed human hypothalamic samples were mounted on a glass slide and incubated overnight at 4 °C with the primary antibody against cellular retinoic acid-binding protein 1 (CRABP1; GTX22816, Gene Tex). The slides were then washed five times with PBS and subsequently incubated for 1 h at room temperature with biotinylated goat anti-mouse IgG (Beyotime Biotechnology, A0126). After three washes, the slides were stained using DAB-peroxidase substrate solution for less than 2 min and visualized using a Nikon Digital Camera.

Fluorescence in situ hybridization

The brains were initially fixed in 4% PFA with poly-glycerol 3-poly-glycidyl ether (P3PE) at 4 °C for 4 h, followed by dehydration through immersion of the slides in graded concentrations of a mixture containing 20% sucrose and P3PE diluted at a ratio of 1:200. Coronal sections measuring 10 μm were obtained from the brains using a Leica cryostat. The RNA in situ detection experiment was conducted using a two-step procedure. During the detection stage, slides were rinsed with DEPC-treated PBS (D-PBS). Pre-hybridization was performed by incubating the slides with probe hybridization buffer for 30 min at 45 °C. To prepare the probe solution, *Sst* probe (1 pmol) and *Cartpt* probe (1 pmol) were added to the hybridization buffer at a temperature of 45 °C. After replacing the pre-hybridization solution with the probe solution, slides were incubated overnight (12–16 h) at 37 °C for probe hybridization. Subsequently, the samples were gently washed using a gradient elution buffer at 37 °C to minimize background noise and ensure accurate detection. This involved sequential elution with wash buffers containing probe concentrations set at levels of 75, 50, and 25%. Finally, the samples were washed twice with elution consisting of 100% 5 × SSCT for a duration of 15 min.

In the amplification stage, prepare 30 pmol of each fluorescently labeled hairpin by snap cooling in 10 μL of 5 × SSC buffer (heat at 95 °C for 90 s and cool to room temperature on the bench top for 30 min). Add all snap-cooled hairpins to the amplification buffer at room temperature. Subsequently, incubate the samples with the hairpin solution for 8 h at room temperature. Following incubation, wash the samples twice with 5 × SSCT at room temperature. Finally, seal the sections with neutral balsam containing DAPI (1 mg/mL), capture photos, and perform analysis.

Hormone stimulation

For administration of hormones directly into the brain, a cannula was placed into the cerebral ventricle. Mice were fixated in a stereotaxic frame, and the scalp was opened to expose the skull. Coordinates were zeroed on bregma and moved to the lateral ventricle (bregma: AP: −0.5 mm, ML: ±1.3 mm, DV: −2.3 mm). A small hole was drilled into the skull and the guide cannula was inserted and fixated. All canulated mice had 1 week to fully recover before being used for any experiments. After recovery, mice received an infusion of hormones via an injector and an infusion pump at a rate of 1 μL/min after recovery. After the infusion, the injector was left for an additional 3 min to avoid backflow. Then, the injector was removed, and mice were monitored for the following studies.

To assess hormone sensitivity, mice were fasted overnight before being intracerebroventricularly (ICV) injected with either vehicle or

https://doi.org/10.1038/s41467-025-57411-7

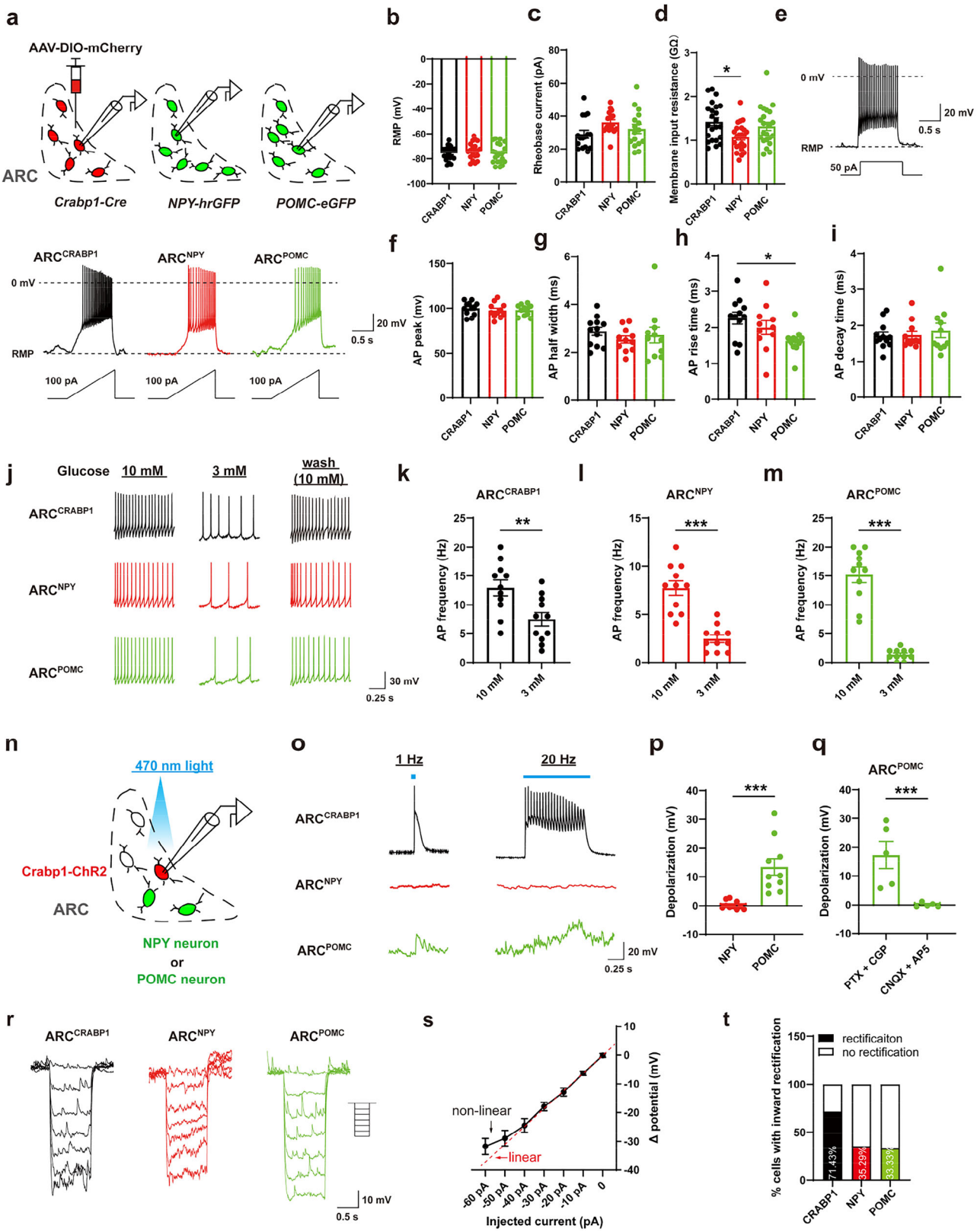

specific hormones. For insulin sensitivity, mice received an injection of insulin (2 mU/mouse; Med Chem Express) and were transcardially perfused with paraformaldehyde 15 min post-injection. For leptin sensitivity, mice were injected with leptin (3 μg/mouse; Med Chem Express) and perfused 45 min later. For ghrelin sensitivity, mice received an injection of ghrelin (1 μg/mouse; Tocris Bioscience) and were perfused 120 min post-injection.

Brain stereotaxical injection of AAV and fiber implantation

Following anesthesia with 1.5–2% isoflurane gas, depending on the weight of the mice, they were positioned in a three-point fixation stereotactic frame. After exposing the skull through a small incision, the skull was aligned between bregma and lambda, and a small hole was drilled for injection. A beveled pulled-glass pipette was inserted into the target regions (300 nL) using a motorized stereotaxic injector

Fig. 6 | Activating ARC^{CRABP1} neurons depolarizes POMC neurons. a Schematic illustration of ARC^{CRABP1}, NPY and POMC neurons labeling and recording strategies (top) and sample images of the electrophysiological responses during 100 pA ramp currents injection in the three types of neurons (bottom). **b**–**d** Electrophysiological indicators, including RMP (**b** ARC^{CRABP1}, $n = 21$, $N = 4$; NPY, $n = 21$, $N = 4$; POMC, $n = 21$, $N = 4$), rheobase current (**c** ARC^{CRABP1}, $n = 16$, $N = 3$; NPY, $n = 16$, $N = 3$; POMC, $n = 16$, $N = 3$) and input resistance (**d** ARC^{CRABP1}, $n = 23$, $N = 4$; NPY, $n = 23$, $N = 4$, $p = 0.0105$ with ARC^{CRABP1}; POMC, $n = 22$, $N = 4$) of the three types neurons. **e** Samples image of the electrophysiological responses during 100 pA ramp current injection in ARC^{CRABP1} neurons. **f**–**i** Some key parameters of AP in ARC^{CRABP1}, NPY and POMC neurons, including AP peak (**f**), half width (**g**), rise time (**h**), and decay time (**i**). (ARC^{CRABP1}, $n = 12$, $N = 3$; NPY, $n = 11$, $N = 3$; POMC, $n = 11$, $N = 3$). **j** Samples images of APs in ARC^{CRABP1}, NPY and POMC neurons under different concentrations of glucose. **k**–**m** Decreased AP frequency in 3 mM ACSF environment of ARC^{CRABP1} (**k** $n = 11$, $N = 3$), NPY (**l** $n = 11$, $N = 3$) and POMC (**m** $n = 11$, $N = 3$) neurons. **n**, **o** Schematic illustration and sample images of ARC^{CRABP1}-ChR2, NPY, and POMC neurons labeling and their responses to 1 and 20 Hz stimuli of 470 nm light. **p**, **q** Opto-activating ARC^{CRABP1} neurons induces the depolarization in POMC neurons (**p** $n = 11$, $N = 3$) and the depolarization can be blocked by CNQX + AP5 (**q** $n = 5$, $N = 2$). **r** Samples image of the electrophysiological responses upon hyperpolarizing stimuli in ARC^{CRABP1}, NPY, and POMC neurons. **s** Quantification of inward rectification to consecutive stimuli as illustrated by the non-linear curve in ARC^{CRABP1} neurons (solid black, $n = 21$, $N = 4$) compared to a theoretical linear curve (red). **t** Percentage of neurons with inward rectification upon hyperpolarization in ARC^{CRABP1} ($n = 21$, $N = 4$), NPY ($n = 17$, $N = 4$), and POMC neurons ($n = 18$, $N = 4$). Data were expressed as mean ± SEM. *n* represents cell number; *N* represents mice number. One-way ANOVA with Sidak's or Tukey's test for panel **b**–**d** and **f**–**i**; Student's *t*-test for panel **k**–**m**, **p**, **q**. $^{*}P < 0.05$, $^{**}P < 0.01$, $^{***}P < 0.001$.

that controlled a Hamilton syringe connected to the glass pipette to achieve an injection rate of 25 nL per minute. The pipette was slowly withdrawn 10 min after injection. All injected mice had 3 weeks to fully recover before being used for any experiments. The coordinates for brain regions were as follows: ARC (bregma: AP: −1.50 mm, ML: ±0.30 mm, DV: −5.90 mm), BNST (bregma: AP: 0.20 mm, ML: ±0.50 mm, DV: −3.50 mm), PVH (bregma: AP: −0.80 mm, ML: ±0.20 mm, DV: −4.80 mm), PBN(bregma: AP: −5.40 mm, ML: ±1.20 mm, DV: −3.35 mm), NTS(bregma: AP: −7.00 mm, ML: ±0.45 mm, DV: −4.50 mm). We employed the following recombinant adeno-associated virus (rAAV) vectors: rAAV-hSyn-DIO-mCherry-WPRE-hGH-pA and rAAV-EF1α-DIO-Caspase3-WPRE-hGH-pA for the ablation experiment; rAAV-hSyn-DIO-hM3D(Gq)-mCherry-WPRE-hGH-pA and rAAV-hSyn-DIO-hM4D(Gi)-mCherry-WPRE-hGH-pA for DREADD experiments; AAV-EF1α-DIO-hChR2(H134R)-mCherry-WPRE-hGH-pA and AAV-EF1α-DIO-eNpHR3.0-mCherry-WPRE-hGH-pA for optogenetic experiments; HSV-ΔTK-LSL-tdTomato, rAAV-EF1α-DIO-EGFP-T2A-TK-WPRE-hGH-pA, rAAV-hSyn-DIO-mGFP-T2A-Synaptophysin-mRuby-WPRE-hGH-PA, CTB 555 (Wuhan Privy Brain Science and Technology Co., Ltd) for tracing experiment. AAV-EF1α-DIO-hChR2(H134R)-mCherry-WPRE-hGH-pA and AAV-*fnpy*-GFP for electrophysiological recording.

Following surgical recovery, an optical fiber with a core diameter of 200 μm and numerical aperture of 0.22 was stereotaxtically inserted into the target regions with its tip positioned above the target areas. Mice implanted with fibers were individually housed to allow one week of recovery before conducting any behavioral experiments. The coordinates of brain regions were as follows: ARC (bregma: AP: −1.50 mm, ML: +0.30 mm, DV: −5.60 mm), BNST (bregma: AP: 0.20 mm, ML: +0.50 mm, DV: −3.20 mm), PVH (bregma: AP: −0.80 mm, ML: +0.20 mm, DV: −4.50 mm), PBN (bregma: AP: −5.40 mm, ML: +1.20 mm, DV: −3.05 mm), NTS (bregma: AP: −7.00 mm, ML: +0.45 mm, DV: −4.20 mm).

In vivo optogenetic studies

The implanted fiber optic cannula was securely attached to a fiber optic cable. Mice were acclimated in experimental cages for one week prior to optogenetic stimulation. For ChR2 and control mice, blue laser light stimulation (473 nm, output power of 5 mW at the tip of the patch cord) consisting of pulse trains (5 ms pulses of 20 Hz; 1 s on, 2 s off) was administered. For NpHR and control mice, yellow laser light stimulation (589 nm, output power of 15 mW at the tip of the patch cord) consisting of pulse trains (5 ms pulses of 20 Hz; 1 s on, 2 s off) was administered. Following a 6-h fasting period, food intake was measured following light stimulation throughout this study. The location of the fiber tip was determined through histology analysis of brain tissue samples. Mice with misplaced fibers outside the target region were excluded from data analysis.

Chemogenetics (DREADD)

Ten-week-old *Crabp1-Cre* male mice received bilateral injections of rAAV-hSyn-DIO-mCherry-WPRE-hGH-pA, rAAV-hSyn-DIO-hM3D (Gq)-mCherry-WPRE-hGH-pA, or rAAV-hSyn-DIO-hM4D (Gi)-mCherry-WPRE-hGH-pA into the ARC. After 3 weeks of recovery from surgery, mice were acclimated in experimental cages for 1 week before chemogenetic stimulation. After a 6-h fasting period, food intake was measured for 4 h following intraperitoneal injection of deschloroclozapine (DCZ, 0.1 mg/kg) in this study. The mice were perfused with PBS, and brains were collected and processed for IHC analysis.

Electrophysiological recording

All recordings were conducted in the ARC region from 3 to 4-month-old male mice. The mouse brains were quickly removed, and coronal brain slices (300 μm) were prepared using a vibrating microtome (Leica, VT1000S) in ice-cold glycerol-based modified artificial cerebrospinal fluid (GaCSF). The GaCSF consisted of the following components (in mM): 244 Glycerol, 2.5 KCl, 2 $MgCl_2$, 2 $CaCl_2$, 1.2 NaH_2PO_4, 10 HEPES, 21 $NaHCO_3$, and 5 Glucose. The pH was adjusted to 7.2 with NaOH and saturated with a mixture of 95% O_2/5% CO_2. The slices were moved to 95% O_2/5% CO_2 saturated ACSF solution, which contained the following concentrations (in mM): 125 NaCl, 2.5 KCl, 1.25 NaH_2PO_4, 25 $NaHCO_3$, 2 $CaCl_2$, 1 $MgCl_2$, 10 D-glucose, 15 D-mannitol, equilibrated with 95% O_2, 5% CO_2, at 28 °C for a minimum duration of 2 h before being transferred to a chamber for recording. The mCherry or EGFP labeled cells were selected for recording based on the expression of the fluorescent marker using the microscope (Olympus BX51WI, Japan) equipped with the appropriate filters and LED light engines (CoolLED-pE100, 470 or 550 nm, UK). Current-clamp recordings of neurons were performed at room temperature and started with the perforated patch-clamp configuration, with glass pipettes (3–4 MΩ) filled with the intracellular solution containing (in mM): 140 K-gluconate, 10 KCl, 10 HEPES, 0.1 EGTA, 2 $MgCl_2$, and 150 μg/mL Amphotericin B (Cat# B1885, APExBIO) (pH 7.25). During the perforation process, the access resistance (Ra) was constantly monitored, and the rectification testing experiments were started when the Ra was stable. After the rectification test, perforated-patch recordings were converted to whole-cell mode, and a ramp current (100 pA, 1 s) or step current (50 pA, 1 s) was injected to induce action potentials. In the glucose sensitivity experiments, D-mannitol was utilized to adjust the osmolarity (310–320 mOsmol) of ACSF, while a 50 pA step current was injected during recording. For the ChR2-assisted experiment, ARC^{CRABP1}, NPY, or POMC neurons were clamped in the current-clamp model, and different frequencies of light (1 s, 473 nm, 4 mW) were delivered from a laser stimulator (Aurora-220, Newdoon, Hangzhou, China) to activate the ChR2-expressing CRABP1 neurons. To investigate the cause of potential alternations in POMC neurons after light stimulation, cells were clamped at -70 mV or 0 mV under the voltage clamp model with the

https://doi.org/10.1038/s41467-025-57411-7

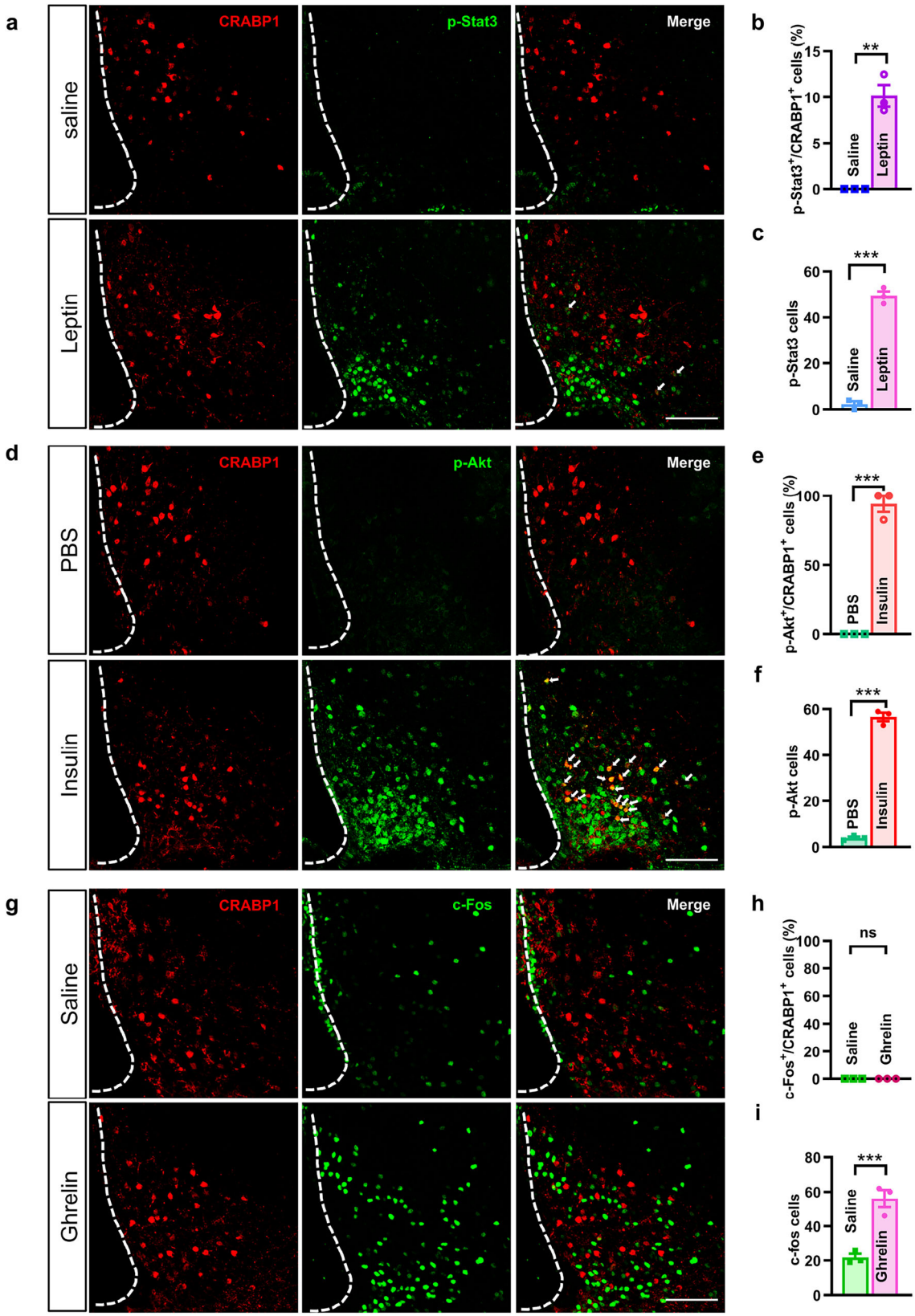

Fig. 7 | Most of ARC^{CRABP1} neurons are activated by insulin stimulation. **a**–**i** Representative confocal images and statistical results depict the immunofluorescence co-localization of CRABP1 with p-Stat3 (**a**–**c**), p-AKT (**g**–**i**), and c-Fos (**d**–**f**) in mice ICV-injected with leptin, ghrelin, or insulin, respectively ($n = 3$, for each condition). Scale bars, 100 μm. CRABP1: red; p-Stat3: green; p-AKT: green; c-Fos: green. n represents mice number. Results are presented as mean ± SEM. Statistic methods: two-tailed Student's t-test. ns represents not significant, $^{*}P < 0.05$, $^{**}P < 0.01$, $^{***}P < 0.001$.

pipette filled with the intracellular solution containing (in mM) 130.0 $CsMeSO_4$, 5.0 NaCl, 1 $MgCl_2$, 0.05 EGTA, 10.0 HEPES, 3.0 Mg-ATP, 0.3 Na_3GTP, and 5.0 QX-314 (pH 7.25). CNQX (10 μM, Cat# N183, Sigma) and AP5 (50 μM, Cat# 0106, Tocris) were employed to exclude glutamatergic synaptic transmission-mediated currents, while Picrotoxin (PTX) (100 μM, Cat# R284556, Sigma) and CGP 52432 (5 μM, Cat# B6655, APExBIO) were utilized to eliminate GABAergic synaptic transmission-mediated currents. For mEPSC recording, cells were clamped at -70 mV under a voltage clamp model with whole-cell recording, and incubated in the ACSF containing 100 μM PTX. During the recordings, cell series resistance was monitored throughout experiments by applying a (−3 mV) step at the end of each sweep, and the experiment was excluded if the resistance changed by more than 20%. All recordings were performed using a Multiclamp 700B patch-clamp amplifier (Molecular Devices, USA), and all data acquisition and analysis were conducted with pCLAMP 10.2 (Molecular Devices, USA) and Mini Analysis software (Synaptosoft, USA). In all electrophysiological experiments, "represents" indicates the number of cells used per animal, typically ranging from three to four cells.

Metabolic analyses

For body weight, food intake, and energy expenditure measures, we did the following experiment. ARC CRABP1 expressing neuron ablation (ACENA) mice and their controls were fed regular chow for a further 10 weeks. Body weight was measured every week. In the first week after recovery, the mice were placed in individual cages and food intake was measured for a whole week.

For energy expenditure (EE) and respiratory exchange ratio (RER) assays, mice at the second week after recovery were individually housed and acclimatized for 48 h in the metabolic cages with ad libitum access to food and water. Next, oxygen consumption (VO_2) and carbon dioxide production (VCO_2) were collected continuously. EE and RER were determined by the following equations: $EE = (3.815 + 1.232 \times RER) \times VO_2$, $RER = VCO_2 / VO_2$.

Body composition analysis was conducted using magnetic resonance imaging (MRI) to determine the ratio of body fat mass to lean mass at Nanjing University of Science and Technology.

Glucose tolerance tests (GTTs) were performed in mice that had been fasted for 12 h overnight. Following the determination of body weights and basal blood glucose concentrations, mice received an intraperitoneal injection of 25% glucose (2 g/kg body weight) between 9 am and 10 am, and blood glucose levels were measured again at 15, 30, 60, and 120 min post-injection. Blood samples for glucose measurement were collected from the tail vein. Glycemia was assessed using a Contour glucometer (Bayer). The glucose response during the glucose tolerance test was calculated by estimating the total area under the glucose curve.

For serum leptin and insulin assays, blood was collected in mice that had been fasted for 12 h overnight and processed to measure serum leptin and insulin levels using a mouse insulin ELISA kit (EZassay, China) and leptin ELISA kit (Crystal Chem Inc., USA), respectively.

For hematoxylin and eosin staining (H&E staining), tissues harvested from mice were fixed in 4% paraformaldehyde (PFA) for 24 h, followed by embedding in paraffin. The tissues were then sectioned at a thickness of 4 μm and stained with hematoxylin and eosin solutions using a standard protocol. Images of subcutaneous white adipose tissue (SC-WAT) adipocytes and liver were captured on a brightfield microscope (Nikon, Japan).

Quantitative RT-PCR

The tissue RNA was extracted using the Trizol lysis solution (9109, Taraka). Complementary RNA was reverse-transcribed to cDNA using HiScript® III RT SuperMix kits (R323-01, Vazyme). RT-PCR was performed on a LightCycler 480 Real-Time PCR System (Roche) using ChamQ SYBR qPCR Master Mix (Q331, Vazyme), in combination with cDNA, primers (Supplementary Table 2), and master mix. The relative expression of genes was analyzed using the $2^{-\Delta Ct}$ method, where ΔCt represents the difference between the Ct value of a given gene and that of the Gapdh control.

Western blotting

The CRABP1 levels were assessed by collecting tissues from C57BL/6J mice, followed by extraction of total proteins using a lysis buffer containing protease and phosphatase inhibitors. Protein concentrations were determined using a BCA protein concentration assay kit (P0009 Beyotime Biotechnology). Subsequently, the protein samples were separated on a 15% SDS-PAGE gel and transferred onto PVDF membranes (Millipore). Western blotting was performed using rabbit-anti-CRABP1 antibody (13163, Cell Signaling Technology) at a dilution of 1:1000, along with mouse-anti-GAPDH antibody (AF0006, Beyotime Biotechnology) at a dilution of 1:1000.

Statistics

Data were presented as either mean ± SEM or individual data points. Statistical analyses were performed using GraphPad Prism to evaluate normal distribution and variations within and among groups. The statistical analyses employed in this study included Student's *t*-test, one-way ANOVA, Two-way ANOVA with Sidewalk's or Tukey's test, two-sided regression-based ANCOVA, or two-tailed Student's *t*-test, as indicated in the respective figure legends. $P < 0.05$ was considered statistically significant.

Reporting summary

Further information on research design is available in the Nature Portfolio Reporting Summary linked to this article.

Data availability

The article and accompanying data include all the empirical evidence that supports the findings presented in this paper. One screenshot of the reference mouse Allen brain atlas (http://atlas.brain-map.org) were used in a Supplementary Fig. The data generated in this study are provided in the Source Data file. Source data are provided with this paper.

References

1. Myers, M. G. Jr., Affinati, A. H., Richardson, N. & Schwartz, M. W. Central nervous system regulation of organismal energy and glucose homeostasis. *Nat. Metab.* **3**, 737–750 (2021).
2. Xu, Y. et al. Distinct hypothalamic neurons mediate estrogenic effects on energy homeostasis and reproduction. *Cell Metab.* **29**, 1232 (2019).
3. Zhang, X. et al. Hypothalamic IKKbeta/NF-kappaB and ER stress link overnutrition to energy imbalance and obesity. *Cell* **135**, 61–73 (2008).
4. Romanov, R. A. et al. Molecular design of hypothalamus development. *Nature* **582**, 246–252 (2020).
5. Betley, J. N., Cao, Z. F., Ritola, K. D. & Sternson, S. M. Parallel, redundant circuit organization for homeostatic control of feeding behavior. *Cell* **155**, 1337–1350 (2013).
6. Alcantara, I. C., Tapia, A. P. M., Aponte, Y. & Krashes, M. J. Acts of appetite: neural circuits governing the appetitive, consummatory, and terminating phases of feeding. *Nat. Metab.* **4**, 836–847 (2022).
7. Dodd, G. T. et al. Leptin and insulin act on POMC neurons to promote the browning of white fat. *Cell* **160**, 88–104 (2015).
8. Krashes, M. J., Lowell, B. B. & Garfield, A. S. Melanocortin-4 receptor-regulated energy homeostasis. *Nat. Neurosci.* **19**, 206–219 (2016).
9. Myers, M. G. Jr. & Olson, D. P. Central nervous system control of metabolism. *Nature* **491**, 357–363 (2012).

10. Steculorum, S. M. et al. AgRP neurons control systemic insulin sensitivity via myostatin expression in brown adipose tissue. *Cell* **165**, 125–138 (2016).
11. Mosialou, I. et al. MC4R-dependent suppression of appetite by bone-derived lipocalin 2. *Nature* **543**, 385–390 (2017).
12. Aponte, Y., Atasoy, D. & Sternson, S. M. AGRP neurons are sufficient to orchestrate feeding behavior rapidly and without training. *Nat. Neurosci.* **14**, 351–355 (2011).
13. De Solis, A. J. et al. Reciprocal activity of AgRP and POMC neurons governs coordinated control of feeding and metabolism. *Nat. Metab.* **6**, 473–493 (2024).
14. Quarta, C. et al. POMC neuronal heterogeneity in energy balance and beyond: an integrated view. *Nat. Metab.* **3**, 299–308 (2021).
15. Chen, R., Wu, X., Jiang, L. & Zhang, Y. Single-cell RNA-seq reveals hypothalamic cell diversity. *Cell Rep.* **18**, 3227–3241 (2017).
16. Napoli, J. L. Cellular retinoid binding-proteins, CRBP, CRABP, FABP5: Effects on retinoid metabolism, function and related diseases. *Pharm. Ther.* **173**, 19–33 (2017).
17. Miyake, T. et al. CRABP1-reduced expression is associated with poorer prognosis in serous and clear cell ovarian adenocarcinoma. *J. Cancer Res. Clin. Oncol.* **137**, 715–722 (2011).
18. Park, S. W. et al. CRABP1 protects the heart from isoproterenol-induced acute and chronic remodeling. *J. Endocrinol.* **236**, 151–165 (2018).
19. Lin, Y. L. et al. CRABP1-CaMKII-Agrn regulates the maintenance of neuromuscular junction in spinal motor neuron. *Cell Death Differ.* **29**, 1744–1756 (2022).
20. Persaud, S. D. et al. All trans-retinoic acid analogs promote cancer cell apoptosis through non-genomic Crabp1 mediating ERK1/2 phosphorylation. *Sci. Rep.* **6**, 22396 (2016).
21. Nagpal, I. & Wei, L. N. All-trans retinoic acid as a versatile cytosolic signal modulator mediated by CRABP1. *Int. J. Mol. Sci.* **20**, 3610 (2019).
22. Lavoie, O. et al. Hypothalamic GABAergic neurons expressing cellular retinoic acid binding protein 1 (CRABP1) are sensitive to metabolic status and liraglutide in male mice. *Neuroendocrinology* **114**, 681–697 (2024).
23. Lin, Y. W., Park, S. W., Lin, Y. L., Burton, F. H. & Wei, L. N. Cellular retinoic acid binding protein 1 protects mice from high-fat diet-induced obesity by decreasing adipocyte hypertrophy. *Int. J. Obes.* **44**, 466–474 (2020).
24. Allen Mouse Brain Atlas. https://mouse.brain-map.org/ (2004).
25. Jais, A. et al. PNOC(ARC) neurons promote hyperphagia and obesity upon high-fat-diet feeding. *Neuron* **106**, 1009–1025 e1010 (2020).
26. Yang, C. F. et al. Sexually dimorphic neurons in the ventromedial hypothalamus govern mating in both sexes and aggression in males. *Cell* **153**, 896–909 (2013).
27. Wang, L. et al. Fasting-activated ventrolateral medulla neurons regulate T cell homing and suppress autoimmune disease in mice. *Nat. Neurosci.* **27**, 462–470 (2024).
28. Jagot, F. et al. The parabrachial nucleus elicits a vigorous corticosterone feedback response to the pro-inflammatory cytokine IL-1beta. *Neuron* **111**, 2367–2382 e2366 (2023).
29. Chen, J. et al. A vagal-NTS neural pathway that stimulates feeding. *Curr. Biol.* **30**, 3986–3998 e3985 (2020).
30. Wang, Y. et al. A bed nucleus of stria terminalis microcircuit regulating inflammation-associated modulation of feeding. *Nat. Commun.* **10**, 2769 (2019).
31. Li, M. M. et al. The paraventricular hypothalamus regulates satiety and prevents obesity via two genetically distinct circuits. *Neuron* **102**, 653–667 e656 (2019).
32. Benevento, M. et al. A brainstem-hypothalamus neuronal circuit reduces feeding upon heat exposure. *Nature* 628:826–834 (2024).
33. Luo, S. X. et al. Regulation of feeding by somatostatin neurons in the tuberal nucleus. *Science* **361**, 76–81 (2018).
34. Silverstein, S. E. et al. A distinct cortical code for socially learned threat. *Nature* **626**, 1066–1072 (2024).
35. Ollivier, M. et al. Crym-positive striatal astrocytes gate perseverative behaviour. *Nature* **627**, 358–366 (2024).
36. Claret, M. et al. AMPK is essential for energy homeostasis regulation and glucose sensing by POMC and AgRP neurons. *J. Clin. Invest.* **117**, 2325–2336 (2007).
37. Morton, G. J., Cummings, D. E., Baskin, D. G., Barsh, G. S. & Schwartz, M. W. Central nervous system control of food intake and body weight. *Nature* **443**, 289–295 (2006).
38. Lopez, M. et al. Hypothalamic fatty acid metabolism mediates the orexigenic action of ghrelin. *Cell Metab.* **7**, 389–399 (2008).
39. Dodd, G. T. et al. A hypothalamic phosphatase switch coordinates energy expenditure with feeding. *Cell Metab.* **26**, 375–393 e377 (2017).
40. Ren, H. et al. FoxO1 target Gpr17 activates AgRP neurons to regulate food intake. *Cell* **149**, 1314–1326 (2012).
41. Koch, M. et al. Hypothalamic POMC neurons promote cannabinoid-induced feeding. *Nature* **519**, 45–50 (2015).
42. Yang, Y., Atasoy, D., Su, H. H. & Sternson, S. M. Hunger states switch a flip-flop memory circuit via a synaptic AMPK-dependent positive feedback loop. *Cell* **146**, 992–1003 (2011).
43. Reis, F. et al. Control of feeding by a bottom-up midbrain-subthalamic pathway. *Nat. Commun.* **15**, 2111 (2024).
44. Garfield, A. S. et al. Dynamic GABAergic afferent modulation of AgRP neurons. *Nat. Neurosci.* **19**, 1628–1635 (2016).
45. Cowley, M. A. et al. The distribution and mechanism of action of ghrelin in the CNS demonstrates a novel hypothalamic circuit regulating energy homeostasis. *Neuron* **37**, 649–661 (2003).
46. Rui, L. Simultaneous targeting of POMC and AgRP neurons. *Nat. Metab.* **6**, 382–383 (2024).
47. Vivot, K. et al. CaMK1D signalling in AgRP neurons promotes ghrelin-mediated food intake. *Nat. Metab.* **5**, 1045–1058 (2023).
48. Atasoy, D., Betley, J. N., Su, H. H. & Sternson, S. M. Deconstruction of a neural circuit for hunger. *Nature* **488**, 172–177 (2012).
49. Chen, Y., Lin, Y. C., Kuo, T. W. & Knight, Z. A. Sensory detection of food rapidly modulates arcuate feeding circuits. *Cell* **160**, 829–841 (2015).
50. Balthasar, N. et al. Divergence of melanocortin pathways in the control of food intake and energy expenditure. *Cell* **123**, 493–505 (2005).
51. Cowley, M. A. et al. Leptin activates anorexigenic POMC neurons through a neural network in the arcuate nucleus. *Nature* **411**, 480–484 (2001).
52. Stuber, G. D. & Wise, R. A. Lateral hypothalamic circuits for feeding and reward. *Nat. Neurosci.* **19**, 198–205 (2016).
53. Dietrich, M. O., Zimmer, M. R., Bober, J. & Horvath, T. L. Hypothalamic Agrp neurons drive stereotypic behaviors beyond feeding. *Cell* **169**, 559 (2017).
54. Rossi, M. A. & Stuber, G. D. Overlapping brain circuits for homeostatic and hedonic feeding. *Cell Metab.* **27**, 42–56 (2018).
55. Jennings, J. H., Rizzi, G., Stamatakis, A. M., Ung, R. L. & Stuber, G. D. The inhibitory circuit architecture of the lateral hypothalamus orchestrates feeding. *Science* **341**, 1517–1521 (2013).
56. Aklan, I. et al. NTS catecholamine neurons mediate hypoglycemic hunger via medial hypothalamic feeding pathways. *Cell Metab.* **31**, 313–326 e315 (2020).
57. Roman, C. W., Derkach, V. A. & Palmiter, R. D. Genetically and functionally defined NTS to PBN brain circuits mediating anorexia. *Nat. Commun.* **7**, 11905 (2016).
58. Cheng, W. et al. NTS Prlh overcomes orexigenic stimuli and ameliorates dietary and genetic forms of obesity. *Nat. Commun.* **12**, 5175 (2021).

59. Day, M. et al. GABAergic regulation of striatal spiny projection neurons depends upon their activity state. *PLoS Biol*. **22**, e3002483 (2024).
60. Tan, H. L. et al. Leptin-activated hypothalamic BNC2 neurons acutely suppress food intake. *Nature* **636**, 198–205 (2024).
61. Friedman, J. M. Leptin and the endocrine control of energy balance. *Nat. Metab*. **1**, 754–764 (2019).
62. Myers, M. G., Cowley, M. A. & Munzberg, H. Mechanisms of leptin action and leptin resistance. *Annu. Rev. Physiol*. **70**, 537–556 (2008).
63. Ruud, J., Steculorum, S. M. & Bruning, J. C. Neuronal control of peripheral insulin sensitivity and glucose metabolism. *Nat. Commun*. **8**, 15259 (2017).
64. Andrews, Z. B. et al. UCP2 mediates ghrelin's action on NPY/AgRP neurons by lowering free radicals. *Nature* **454**, 846–851 (2008).
65. Zhao, Y. et al. Gastric mechanosensitive channel Piezo1 regulates ghrelin production and food intake. *Nat. Metab*. **6**, 458–472 (2024).

Acknowledgements

This study received financial support from various sources, including the Noncommunicable Chronic Diseases-National Science and Technology Major Project (2024ZD0530203), National Natural Science Foundation of China (grant numbers 81570774, 82070872, 92049118, and 82370854), the Junior Thousand Talents Program of China, and the Nanjing Medical University Startup Fund (All awarded to J.L.). We would also like to acknowledge the support provided by Jiangsu Province's Innovation Personal as well as Innovative and Entrepreneurial Team of Jiangsu Province (Grant No. JSSCTD2021) (All awarded to J.L.), STI2030-Major Project (2021ZD0201100) Task 4 (2021ZD0201104) (awarded to Y.Z.), Jiangsu Province Traditional Chinese Medicine Science and Technology Development Program (MS2023087) (awarded to G.Z.), and Fund of Biological and Medical Sciences of Applied Summit Nurturing Disciplines in Anhui Province (202313) (awarded to Q.C.). We express our gratitude to Dr. Sheng Yang from the School of Public Health at Nanjing Medical University for his valuable review of our statistical data.

Author contributions

L.Y. and X.Z. made equal contributions to this study. J.L. conceived and designed the study while L.Y., X.Z., A.L., and Q.J. conducted experiments and analyzed data. L.J., Y.L., Y.C., J.Z., Z.S., J.Q., C.Q., G.D., and Y.Z. performed experimental procedures. The manuscript was written by J.L. with input from L.Y. and A.L. A.L. and Q.J. revised the manuscript and provided valuable comments on the manuscript.

Competing interests

The authors declare no competing interests.

Additional information

Supplementary information The online version contains supplementary material available at https://doi.org/10.1038/s41467-025-57411-7.

Correspondence and requests for materials should be addressed to Qin Jiang, An Liu or Juxue Li.

Peer review information *Nature Communications* thanks the anonymous reviewers for their contribution to the peer review of this work. A peer review file is available.